International Journal of Electrical and Electronic Science
2018; 5(2): 33-38
http://www.aascit.org/journal/ijees
ISSN: 2375-2998

AASCIT American Association for Science and Technology

Comparative Electrostatics of Radial *p-n* Heterojunctions with Opposite Sequences of the Layers

Vitalii Borblik

Department of Electrical & Galvanomagnetic Properties of Semiconductors, Institute of Semiconductor Physics, Kiev, Ukraine

Email address

borblik@isp.kiev.ua

Citation

Vitalii Borblik. Comparative Electrostatics of Radial *p-n* Heterojunctions with Opposite Sequences of the Layers. *International Journal of Electrical and Electronic Science.* Vol. 5, No. 2, 2018, pp. 33-38.

Received: February 27, 2018; **Accepted**: March 21, 2018; **Published**: May 10, 2018

Abstract: Electrostatics of radial core-shell heterostructure *p-n* junctions is considered theoretically in two combinations: narrow-bandgap core/wide-bandgap shell and vice versa. Because of cylindrical symmetry of the structure, depletion width of the core increases with decrease of the interface radius but depletion width of the shell, on the contrary, decreases. Thereby the relative contribution from different materials into performance characteristics of devices, which use a heterostructure *p-n* junction, changes substantially. Sequence of the different layers is of importance as well. In both combinations, values of depletion widths in the heterostructure *p-n* junction prove to be intermediate between those for homostructure *p-n* junctions made of the constituent materials at the same doping levels. Analogous situation takes place for barrier capacitance of the heterostructure *p-n* junction.

Keywords: Core-shell Nanowire, Heterostructure, *p-n* Junction, Depletion Width, Barrier Capacitance

1. Introduction

Semiconductor nanowires are widely researched as potential building blocks for nanoelectronic circuits. In particular, special attention to multilayer nanowires is given. Thus, for example, the coaxial *p-n* and *p-i-n* nanostructures are proposed for fabrication of advanced types of solar cells [1]. In this case, light may fall in axial direction of the nanowire that provides complete light absorption but separation of the photo-excited electron-hole pairs occurs in perpendicular, radial, direction. Extent of the structure in this direction may be shorter than diffusion length of the minority carriers in the most defective material. This allows reducing requirements to the device material quality and makes it cheaper.

In order to enhance performance of such the devices, *p*- and *n*-layers are made sometimes of different materials: CdS/Cu_2S [2], GaAs/InGaAs [3], ZnO/Si [4]. This allows enlargement of the built-in potential.

On the base of longitudinal carrier transport in such structures, along an axis of the nanowire, the core-shell heterostructures are considered as high performance field-effect transistors [5] as well as high electron mobility devices [6]. And on the base of lateral transport, the radial heterostrucrure tunnel diodes [7], core-multishell high-efficiency light-emitting diodes [8], and coaxial core-shell nanowire lasers [9] have been demonstrated. However theory of such radial heterojunctions is absent practically.

Theory of planar semiconductor heterojunctions is well known - see, for example, the book of B. L. Sharma and R. K. Purohit [10]. The heterojunctions are differentiated on type (I- or II-type, depending on relative arrangement of the energy bands for constituent materials) and on doping character (isotype or anisotype).

As was shown in papers [11-14], cylindrical symmetry of radial *p-n* homojunctions changes their electrostatics sufficiently. In particular, all the characteristics become dependent on the junction radius. It is of interest to study the same problem for heterostrucrure radial *p-n* junctions where a new parameter appears – the energy band discontinuity.

2. Theory

A radial *p-n* hetero-diode made of different materials 1 and 2 with partially depleted *p*- and *n*-regions is shown

schematically in Figure 1 where r_0 is the interface radius, r_p is the depletion region boundary in the core, and r_n is the depletion region boundary in the shell.

In the depletion approximation, profile of the potential V is determined by Poisson equations for two regions

$$\frac{1}{r}\frac{d}{dr}\left(r\frac{dV_1}{dr}\right)=\frac{qN_{A1}}{\varepsilon_1},\ r_p \le r \le r_0, \tag{1}$$

$$\frac{1}{r}\frac{d}{dr}\left(r\frac{dV_2}{dr}\right)=-\frac{qN_{D2}}{\varepsilon_2},\ r_0 \le r \le r_n, \tag{2}$$

where N_{A1} and N_{D2} are the acceptors and donors concentrations, respectively, ε_1 and ε_2 are the dielectric constants of two materials.

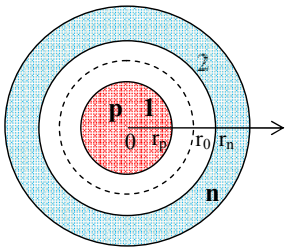

Figure 1. *Schematic view of the radial p-n heterostructure.*

Matching the electric inductions at the interface r_0 gives equation

$$N_{A1}\left(r_0^2-r_p^2\right)=N_{D2}\left(r_n^2-r_0^2\right) \tag{3}$$

and matching the potentials results in equation

$$\frac{qN_{A1}}{2\varepsilon_1}\left(\frac{r_0^2-r_p^2}{2}+r_p^2\ln\frac{r_p}{r_0}\right)+\frac{qN_{D2}}{2\varepsilon_2}\left(\frac{r_0^2-r_n^2}{2}+r_n^2\ln\frac{r_n}{r_0}\right)=V_{bi} \tag{4}$$

where V_{bi} is the total built-in potential. Ratio of the partial built-in potentials V_{b1} and V_{b2} connected with depletion widths of the core and the shell is

$$\frac{V_{b1}}{V_{b2}}=\frac{\frac{N_{A1}}{\varepsilon_1}\left(\frac{r_0^2-r_p^2}{2}+r_p^2\ln\frac{r_p}{r_0}\right)}{\frac{N_{D2}}{\varepsilon_2}\left(\frac{r_0^2-r_n^2}{2}+r_n^2\ln\frac{r_n}{r_0}\right)}=\frac{N_{A1}\varepsilon_2}{N_{D2}\varepsilon_1}\frac{\frac{1}{2}\left(1-\frac{r_p^2}{r_0^2}\right)+\frac{r_p^2}{r_0^2}\ln\frac{r_p}{r_0}}{\frac{1}{2}\left(1-\frac{r_n^2}{r_0^2}\right)+\frac{r_n^2}{r_0^2}\ln\frac{r_n}{r_0}} \tag{5}$$

System of equations (3)-(4) can be solved only numerically. Expressing r_n in terms of r_p from (3)

$$r_n=\sqrt{r_0^2+\left(r_0^2-r_p^2\right)N_{D2}/N_{A1}} \tag{6}$$

one obtains transcendental equation in r_p

$$\frac{N_{A1}}{2N_{D2}}\left(\frac{\varepsilon_2}{\varepsilon_1}-1\right)\left(1-\frac{r_p^2}{r_0^2}\right)+\frac{N_{A1}\varepsilon_2}{N_{D2}\varepsilon_1}\frac{r_p^2}{r_0^2}\ln\frac{r_p}{r_0}+\left[1+\frac{N_{A1}}{N_{D2}}\left(1-\frac{r_p^2}{r_0^2}\right)\right]\ln\sqrt{1+\frac{N_{A1}}{N_{D2}}\left(1-\frac{r_p^2}{r_0^2}\right)}-\frac{V_{bi}2\varepsilon_2}{qN_{D2}r_0^2}=0 \tag{7}$$

At $\varepsilon_1=\varepsilon_2$ this equation reduces to that for radial *p-n* homojunction [14]. Under bias conditions V_{bi} has to be replaced by $V_{bi}-U$, V_{b1} - by $V_{b1}-U_1$, and V_{b2} - by $V_{b2}-U_2$ where $U=U_1+U_2$ is the applied voltage.

In order to solve Eq. 7 it is necessary to know value of V_{bi}.

Here we consider abrupt anisotype *p-n* heterojunction of the type I for which energy band scheme (before bringing two materials into contact) have a form shown in Figure 2 for two material combinations: narrow-bandgap core/wide-bandgap shell (a) and vice versa (b).

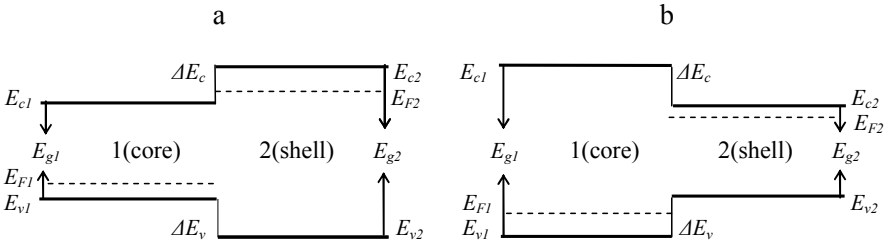

Figure 2. *Energy bands arrangement of type I for p-n heterojunctions; here E_{c1} and E_{c2} are bottoms of the conductivity bands, E_{v1} and E_{v2} are tops of the valence bands, ΔE_c and ΔE_v are the energy bands discontinuities, E_{g1} and E_{g2} are the energy gaps, E_{F1} and E_{F2} are the Fermi levels.*

Under conditions of the non-generated semiconductors, the following expressions take place

$$E_{F1} - E_{v1} = kT \ln \frac{N_{v1}}{N_{A1}}, \quad (8)$$

$$E_{c2} - E_{F2} = kT \ln \frac{N_{c2}}{N_{D2}}, \quad (9)$$

where N_{v1} and N_{c2} are the effective densities of states in the valence and conduction bands, respectively. Adding (8) and (9) gives

$$qV_{bi} \equiv E_{F2} - E_{F1} = E_{c2} - E_{v1} - kT \ln\left(\frac{N_{v1}N_{c2}}{N_{A1}N_{D2}}\right). \quad (10)$$

In the first combination (a) this comes to

$$qV_{bi} = E_{g1} + \Delta E_c + kT \ln\left(\frac{N_{A1}N_{D2}}{N_{v1}N_{c2}}\right) \quad (11)$$

and in the second one (b) - to

$$qV_{bi} = E_{g1} - \Delta E_c + kT \ln\left(\frac{N_{A1}N_{D2}}{N_{v1}N_{c2}}\right). \quad (12)$$

In concordance with Anderson's [15] "electron affinity rule" $\Delta E_c = \chi_1 - \chi_2$ where χ_1 and χ_2 are the electron affinities of two materials.

The barrier capacitance $C = \frac{dQ_p}{dU}$ where Q_p is the electron charge concentrated in depleted *p*-region of the heterojunction and given by

$$Q_p = qN_{A1}\pi\left(r_0^2 - r_p^2\right)L \quad (13)$$

where r_p is *U*-dependent and L is length of the nanowire. Inasmuch as

$$\frac{dr_p}{dU} = \frac{\varepsilon_2}{qN_{A1}r_p}\left[\frac{\varepsilon_2}{\varepsilon_1}\ln\frac{r_p}{r_0} - \ln\sqrt{1 + \frac{N_{A1}}{N_{D2}}\left(1 - \frac{r_p^2}{r_0^2}\right)}\right]^{-1} \quad (14)$$

the capacitance per unit area of the *p-n* junction is

$$C = \frac{2\varepsilon_1\varepsilon_2}{r_0}\left[\varepsilon_1 \ln\left(\frac{r_n}{r_0}\right)^2 - \varepsilon_2 \ln\left(\frac{r_p}{r_0}\right)^2\right]^{-1}. \quad (15)$$

At $\varepsilon_1 = \varepsilon_2$ Eq. 15 reduces to corresponding expression for homojunction [12].

3. Numerical Results

The numerical calculations are performed for radial hetero-diodes *p*-Ge/*n*-GaAs and *p*-GaAs/*n*-Ge because this heteropair has good lattice match conditions i.e. no appreciable density of interface states can be associated with this heterojunction.

In accordance with the data from [10], in this case ΔE_c= 4.13 eV–4.07 eV= 0.06 eV. Corresponding value $\Delta E_v = \Delta E_g - \Delta E_c$ = (1.42-0.66) eV- 0.06 eV= 0.7 eV. The densities of states for Ge and GaAs as well as values of the energy gaps are taken from [16].

3.1. The Depletion Widths

Figure 3 represents the calculated depletion widths $w_p = r_0 - r_p$ and $w_n = r_n - r_0$ of the core and shell, respectively, as a function of the interface radius r_0 for both heterodiodes at $N_{A1} = N_{D2} = 10^{18} cm^{-3}$ (solid curves). It is seen that when the interface radius decreases, depletion width of the core increases and depletion width of the shell, on the contrary, decreases. This is the consequence of cylindrical symmetry of the structure when the solutions of differential equations are characterized by radial falling. This is the reason why the built-in electric field of the *p-n* junction which is maximal at its metallurgical boundary decays in direction of the shell faster than it does in direction of the core. In paper [17], analogous effect has manifested itself in radial distributions of injected carriers: their concentration decayed in direction of the shell faster than it did in direction of the core.

For comparison, the corresponding results for *p-n* homojunctions in Ge (dash-dot) and GaAs (dash-dot-dot) at the same impurity concentrations are shown in Figure 3 as well.

Above values of ΔE_c (and ΔE_v) are not commonly accepted. Theoretical values from different authors as well as experimentally measured energy band discontinuities differ, as a rule, appreciably. In scientific literature, the valence band discontinuities are given usually [18, 19]. For Ge/GaAs heteropair, experimental and theoretical values of this quantity are scattered in the interval from 0.25 to 0.71 eV. Therefore Figure 3 demonstrates also the calculation results corresponding to the case of minimal ΔE_v = 0.25 eV (thereafter, maximal ΔE_c = 0.51 eV) at the same doping levels (dash curves). It is obviously that in the heterodiodes of both types, depletion widths of the heterojunction are situated between corresponding values for homojunctions made of the constituent materials at any value of the band discontinuities (shaded areas between solid and dash curves). Furthermore, above mentioned areas are located, as a whole, closer to the value for core material.

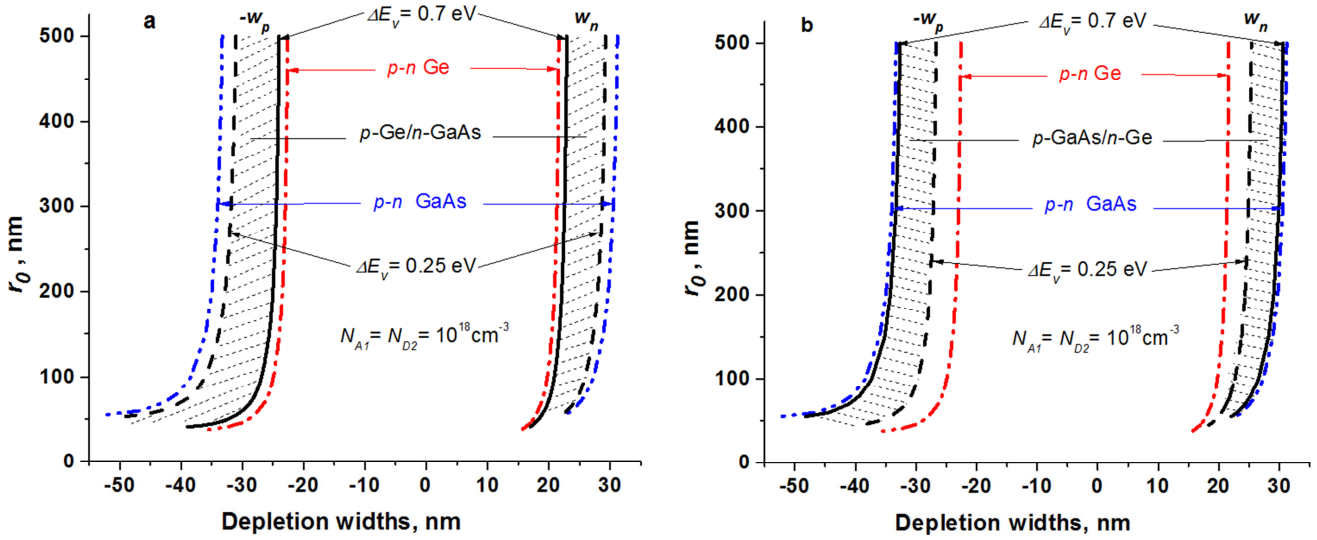

Figure 3. *Dependences of the depletion widths of the core w_p and shell w_n on radius of the core-shell interface at $N_{A1} = N_{D2} = 10^{18}$ cm^{-3} in the heterodiodes (a)- and (b)-types (an abscissa equal to zero corresponds to the interface); solid and dash curves - for the valence band discontinuity of ΔE_v =0.7 and 0.25 eV, respectively; dash-dot and dash-dot-dot curves – the same for Ge and GaAs p-n homojunctions, respectively.*

Figure 4 represents r_0-dependences of the whole depletion widths $w = w_p + w_n$ of both heterodiodes in all range of ΔE_v values. It is seen that w for the diode with GaAs core (area with dash shading), in whole, larger than that for the diode with Ge core (solid shading).

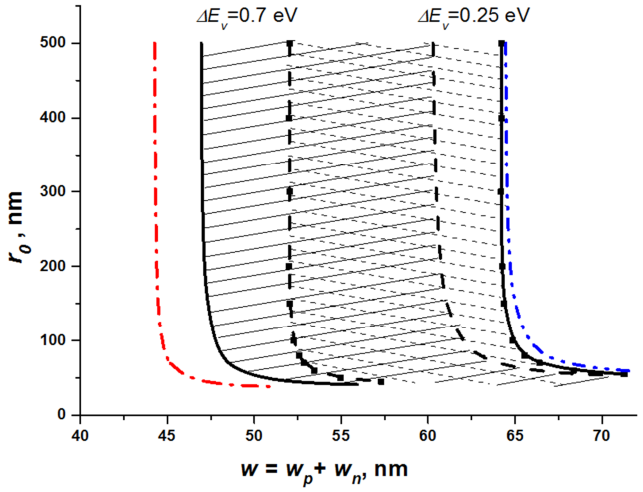

Figure 4. *Dependences of the whole depletion width w on radius of the core-shell interface in the heterodiode (a)-type (solid and dash lines) and in the heterodiode (b)-type (solid and dash lines with symbols) in all range of ΔE_v values at $N_{A1} = N_{D2} = 10^{18}$ cm^{-3}; dash-dot and dash-dot-dot lines refer to p-n homojunctions in Ge and GaAs, respectively, at the same impurity concentrations.*

3.2. The Partial Built-in Potentials of the Core and Shell

The built-in potentials of the core and shell each taken separately, depend on heterojunction radius as well. In Figure 5 such dependences are represented for both the heterodiodes at equilibrium (U=0).

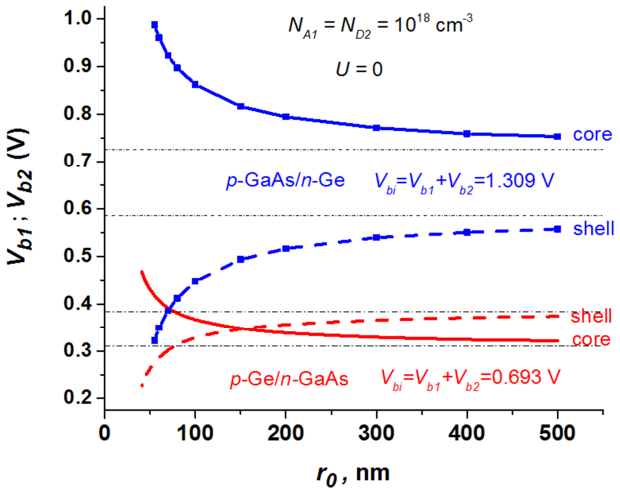

Figure 5. *Dependences of the partial built-in voltages V_{b1} (solid curves) and V_{b2} (dash) on radius of the core-shell interface; results for the heterodiode (a)-type are shown as lines and those for the heterodiode (b)-type - as lines with symbols; ΔE_v = 0.7 eV.*

It is seen that the built-in voltage of the core increases and that of the shell decreases with decreasing in the interface radius r_0 in accordance with analogous behavior of the depletion widths. In the limit of large radiuses, the results go to those for planar hetero-diodes.

3.3. The Barrier Capacitance

Figure 6 presents dependences of $1/C^2$ versus applied voltage for heterojunctions of (a)- and (b)-types and for *p-n* homojunctions made of Ge or GaAs at different values of interface radius. At the large radius, these dependences are close to linier ones but more and more deviate from them with decreasing in r_0. At any value of r_0, the voltage dependences of $1/C^2$ for heterojunctions are situated

between corresponding dependences for homojunctions made of the constituent materials taken at the same doping levels. But they are located closer to corresponding values for *p-n* diode made of core material.

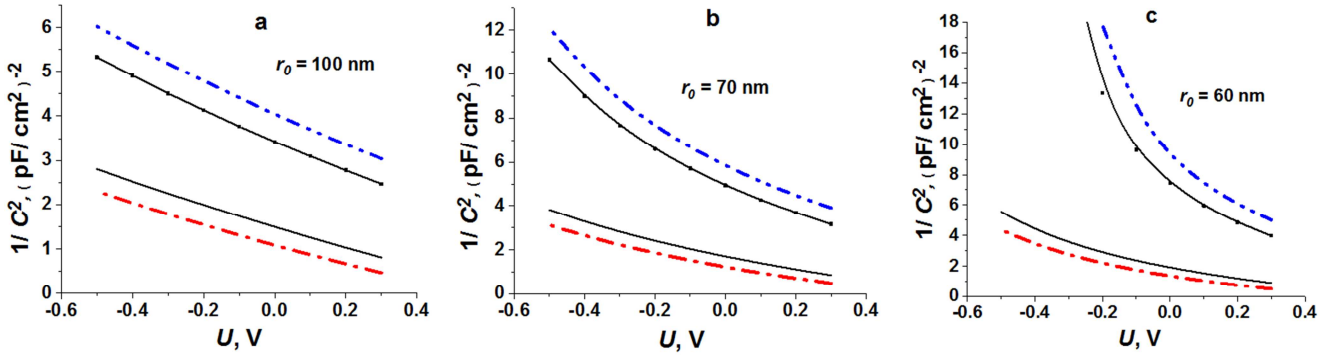

Figure 6. *Dependences of* $1/C^2$ *on applied voltage in p-Ge/n-GaAs heterojunction (solid lines), in p-GaAs/n-Ge heterojunction (solid lines and symbols), in Ge p-n homojunction (dash-dot lines), and in GaAs p-n homojunction (dash-dot-dot) at interface radius of 100 nm (a), 70 nm (b), and 60 nm (c) and the same impurities concentrations* $N_{A1} = N_{D2} = 10^{18}$ *cm*$^{-3}$ *(*ΔE_v *=0.7 eV).*

4. Conclusions

Thus the depletion widths of the core and the shell in radial *p-n* heterojunction at any sequence of *p*- and *n*-layers prove to be intermediate between those in the homojunctions made of the constituent materials at the same doping levels. The same concerns also the barrier capacitance. The whole depletion width of the heterojunction is larger in the heterodiode with core made of more wide-bandgap semiconductor.

Increase in the core depletion width with decreasing in the interface radius and concurrent decrease in depletion width of the shell can be important in such devices as solar cell because this results in change of relative contribution to device performance characteristics from different materials constituting the heterojunction.

Acknowledgements

This work was supported by the National Academy of Sciences of Ukraine (project III-10-15).

Conflicts of Interest

The author declares that there are no conflicts of interest regarding the publication of this paper.

References

[1] B. Tian, X. Zheng, T. J. Kempa, Y. Fang, N. Yu, G. Yu, J. Huang, and C. M. Lieber, Coaxial silicon nanowires as solar cells and nanoelectronic power sources, *Nature*, vol. 449, pp. 885-890, 2007.

[2] J. Tang, Z. Huo, S. Brittman, H. Gao, and P. Yang, Solution-processed core–shell nanowires for efficient photovoltaic cells, *Nature Nanotechnology*, vol. 6, pp, 568-572, 2011.

[3] K. Moratis, S. L. Tan, S. Germanis, C. Katsidis, M. Androulidaki, K. Tsagaraki, Z. Hatzopoulos, F. Donatini, J. Cibert, Y.-M. Niquet, H. Mariette, and N. T. Pelekanos, Strained GaAs/InGaAs core-shell nanowires for photovoltaic applications, *Nanoscale Research Letters,* vol. 11, no. 176, 2016.

[4] I. T. Yoon, H. D. Cho, H. Y. Cho, D. W. Kwak, and S. Lee, Effect of Si growth temperature on fabrication of Si-ZnO coaxial nanorod heterostructure on (100) Si substrate, *J. Electron. Mater*, vol. 46, no. 7, pp. 4119-4125, 2017.

[5] J. Xiang, W. Lu, Y. Hu, Y. Wu, H. Yan, and C. M. Lieber, Ge/Si nanowire heterostructures as high-performance field-effect transistors, *Nature,* vol. 441, pp. 489-493, 2006.

[6] X. Jiang, Q. Xiong, S. Nam, F. Qian, Y. Li, and C. M. Lieber, InAs/InP radial nanowire heterostructures as high electron mobility devices, *Nano Lett*. Vol. 7, no. 10, pp. 3214-3218, 2007.

[7] O. Tizno, B. Ganjipour, M. Heurlin, C. Thelander, M. T. Borgstrom, and L. Samuelson, Radial tunnel diodes based on InP/InGaAs core-shell nanowires, *Appl. Phys. Lett.,* vol. 110, 113501, 2017.

[8] F. Qian, S. Gradečak, Y. Li, C.-Y. Wen, and C. M. Lieber, Core/multishell nanowire heterostructures as multicolor, high-efficiency light-emitting diodes, *Nano Lett.*, vol. 5, no. 11, pp. 2287-2291, 2005.

[9] B. Hua, J. Motohisa, Y. Kobayashi, S. Hara, and T. Fukui, Single GaAs/GaAsP coaxial core-shell nanowire lasers, *Nano Lett.*, vol. 9, no. 1, pp. 112-116, 2009.

[10] B. L. Sharma and R. K. Purohit, *Semiconductor Heterojunctions*, Pergamon Press, 1974.

[11] B. M. Kayes, H. A. Atwater, and N. S. Lewis, Comparison of the device physics principles of planar and radial p-n junction nanorod solar cells, *J. Appl. Phys.,* vol. 97, 114302, 2005.

[12] S. Petrosyan, A. Yesayan, and S. Nersesyan, Theory of nanowire radial p-n-junction, World Acad. Sci. Eng. Technol., vol. 71, pp. 1065-1070, 2012.

[13] A. C. E. Chia and R. R. LaPierre, Electrostatic model of radial pn junction nanowires, *J. Appl. Phys.,* vol. 114, 074317, 2013.

[14] V. L. Borblik, Concerning the depletion width of a radial *p-n* junction and its influence on electrical properties of the diode, *Semiconductor Physics, Quantum Electronics & Optoelectronics,* vol. 20, no. 2, pp. 168-172, 2017.

[15] R. L. Anderson, Experiments on Ge-GaAs heterojunctions, Solid-State Electronics, vol. 5, no. 5, pp. 341-351, 1962.

[16] S. M. Sze, *Physics of Semiconductor Devices,* 2nd edn. John Wiley & Sons, New York – Chichester – Brisbane – Toronto – Singapore, 1981.

[17] V. Borblik, Effect of circular p-n junction curvature on the diode current density, *J. Electron. Mater.*, vol. 45, no. 8, pp. 4117-4121, 2016.

[18] J. Pollmann and A. Mazur, Theory of semiconductor heterojunctions, *Thin Solid Films,* vol. 104, no. 3-4, pp. 257-276, 1983.

[19] W. Pollard, Valence-band discontinuities at semiconductor heterojunctions, *J. Appl. Phys.,* vol. 69, no. 5, pp. 3154-3158, 1991.